ACS APPLIED MATERIALS & INTERFACES

www.acsami.org

Research Article

Self-Enriching Electrospun Biosensors for Impedimetric Sensing of Zika Virus

Isaac A. M. Frias, Laura Helena Vega Gonzales Gil, Marli T. Cordeiro, Maria D. L. Oliveira, and Cesar A. S. Andrade*

Cite This: *ACS Appl. Mater. Interfaces* 2022, 14, 41−48

Read Online

ACCESS | Metrics & More | Article Recommendations | Supporting Information

ABSTRACT: Zika virus (ZIKV) infection is associated with the Guillain−Barré syndrome, and when non-vector congenital transmission occurs, fetal brain abnormalities are expected. After ZIKV infection, the blood, breast milk, and other body fluids contain low viral loads. Their detection is challenging as it requires the processing of larger input volumes of the clinical samples. Pre-enrichment is a valuable strategy to increase the analyte concentration. Therefore, the authors propose the use of a hierarchal composite polyaniline-(electrospun nanofiber) hydrogel mat (ENM) for the simultaneous enrichment and impedimetric sensing of ZIKV viral particles. The electrospinning conditions of polyvinyl alcohol and alginate, including blend formulation, were optimized through a factorial design. Disintegration and gelatinization were controlled *via* cross-linking to improve the hydrogel properties. Hierarchization was achieved by *in situ* chemical deposition of conductive polyaniline. The carboxyl groups of the ENM were used for the covalent immobilization of anti-ZIKV polyclonal antibodies used in the specific recognition of ZIKV within the medium of Vero cell culture. The specific capture and desorption of virions were studied at different pHs. ENMs were characterized by scanning electron microscopy and FTIR. Atomic force microscopy along with UV−vis and electrochemical impedance spectroscopies was used to monitor the antibody immobilization, ZIKV capture, and elution processes. Our results show that 14.2 mg (0.25 cm^3) of ENM can capture 38.7 ± 2.5 μg of ZIKV with a desorption rate of 99.97% (38.29 ± 2.7 μg ZIKV), which is reusable for at least three times. Therefore, the capture capacity (micrograms of ZIKV captured per milligram of ENM) of polyaniline-hierarchized mats was 2.72 μg ZIKV/mg. The impedance LOD value was determined to be 2.76 μg of ZIKV particles (approximately 6.6 × 103 PFU/mL). As a result, we present a fast small-scale purification system that can simultaneously monitor ZIKV electrochemically and optically.

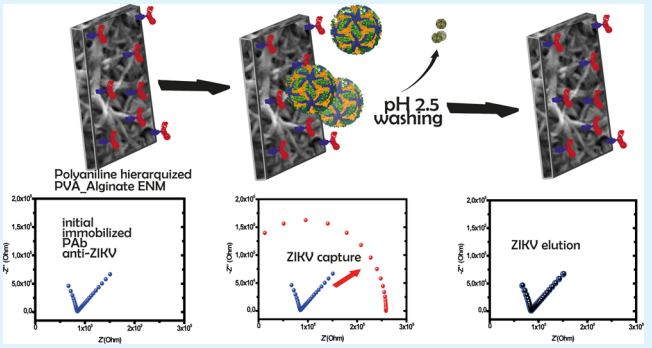

KEYWORDS: *electrochemical biosensor, ZIKV, viral detection, electrospun nanofibers, label-free detection, polyaniline*

1. INTRODUCTION

Zika virus (ZIKV) is an arbovirus of the family *Flaviviridae* and genus Flavivirus with a single-stranded positive-sense RNA and a genome containing 10,794 nucleotides.[1] Its name is eponymous to the Ugandan forest, where it was first identified in 1947 in a sentinel rhesus monkey (*Macaca mulatta*) by a yellow wild fever surveillance network. The RNA of ZIKV translates into a single polyprotein containing envelope, structural, and non-structural proteins. During natural infection, the polyclonal antibodies target NS1 and NS2; however, the envelope remains the main target of humoral response, particularly the third domain (EDIII).[2] It is possible to detect ZIKV RNA in the blood, urine, saliva, nasopharynx samples,[3] and amniotic fluids[4] by using complex extraction protocols and qRT-PCR. However, to provide broad and fast diagnostics, serological methods are more practical in terms of simplicity, readiness, and cost. Nonetheless, their development is mainly challenged by the existence of a cross-reaction among the antibodies raised by different flavivirus infections and the lack of sufficient immune response during the initial contagious phase.[5]

IgM diagnostic kits detect antibodies in the acute phase of infection, while IgG antibodies allow postinfection diagnosis. However, it is known that even in optimal conditions, obtaining results depends on the availability of trained personnel to perform the clinical laboratory routine, which usually takes at least 24 h. Of note, there is a cross-reaction of ZIKV (*Flaviviridae*, Flavivirus, from the Spondweni group) with DENV (*Flaviviridae*, Flavivirus, from the Dengue group)

Received: July 24, 2021
Accepted: December 6, 2021
Published: December 21, 2021

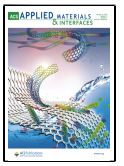

but not with CHIKV since it belongs to another taxonomic genus (*Alphavirus*, family Togaviridae).[6] Antibodies obtained *via* the plaque reduction neutralization test (PRNT) may be more specific than ELISA detection of IgM in the case of primary ZIKV infection. However, they can also present indeterminate results, either for cases of secondary infection, for patients who have already been exposed to other flaviviruses, for residents in areas where these viruses co-circulate, or for those who have received vaccination against another virus of the same family.[7] Individuals suspected of primary ZIKV infection but have already been infected with DENV can be positive for IgM or other neutralizing antibodies against ZIKV.[8] In fact, in mid-2015, a patient from Colombia was diagnosed with multiple infections by DENV, ZIKV, and CHIKV.[9] However, these results were revised in January 2016.[10] After that, it was recommended to interpret the serological diagnosis of patients based on the endemic and epidemic dynamics of the most probable region where contamination occurred in each case.

Since the last outbreak, several biosensors for early detection of ZIKV infection have been reported, including genosensors, immunosensors, and aptasensors.[11] Nanostructured transducers stand out for enabling biosensors with lower limits of detection and better selectivity than traditional assays. In fact, detection attains clinical significance levels, but the diagnosis of real samples is still challenging.[12] Although biosensor sensitivity may be increased by providing more active sites, to improve the sensitivity in clinical samples, purification and preconcentration methods must be optimized by using larger input volumes of the clinical samples.[13]

Electrochemistry can be used for biomedical applications and microbial electrochemical systems (MESs) to study single molecular events or bulk ion transport across a sensor surface. For these applications, three-dimensional (3-D) open-porous transducing materials have shown superior performance and play an important role contributing to high biocompatibility, surface area, conductivity, and low cost.[14] For instance, 3-D electrodes fabricated from metal oxides dispersed in carbon foam[15] and activated carbon fibers impregnated with metal oxide nanoparticles[16] are some of the interesting materials used to accomplish bioelectricity and biocatalysis applications. 3-D nanoporous anodic alumina was employed for the fluorescent determination of trypsin.[17] Multilayered polystyrene nanospheres hierarchized with PEDOT/gold nanoparticles have been used for miRNA biosensing.[18] Also, hydrogel scaffolds were used for electrochemiluminescent biosensing of xanthine.[19] In this application, we found that electrospinning allows the formation of one-dimensional nanostructured fibers. The accumulation of electrospun nanofibers builds up a 3-D porous membrane with a sizable area−volume ratio.[20] In this manner, polycaprolactone nanofibers have been used as a reaction membrane for lateral flow assay detection of ZIKV DNA.[21] However, electrospunnable formulations require essential characteristics to form a continuous fiber while simultaneously avoiding spinneret clogging. Their remarkable interaction with water limits applications with biocompatible polymers. For instance, the rapid expansion of wet alginate prevents it from being electrospun. On the other hand, wetting of polyvinyl alcohol (PVA)-electrospun fibers results in instant disintegration.

Some researchers have tried to control their hygroscopic properties by adding hard cross-linkers to the mixture, such as boric acid and calcium chloride[22] or synthetic clays.[23] However, these treatments hinder functional groups, thus limiting their utilization in specific capture processes. Of note, these kinds of materials are usually employed as coatings and microcapsules.[24] A recent study proposed substrates of similar polymeric blends to promote cellular growth and proliferation, but their aqueous instability prevented their usability.[25] Additionally, functional groups can be favored by adding natural polymers, polymer blends, or biomolecules. Cellulose-electrospun nanofibers functionalized with protein A/G have been used as affinity membranes for unspecific purification of immunoglobulins.[26]

In this work, we prepared a blend to be used in the low-cost electrospinning of biocompatible materials such as alginate and highly hygroscopic PVA to fabricate electrospun nanofiber mats (ENMs). Alcoholic glutaraldehyde cross-linking treatment was performed to promote its stabilization toward water, which allowed the formation of an open-porous characteristic and *in situ* chemical deposition of conductive polyaniline. The remaining carboxyl groups were used to tether anti-ZIKV PAbs. Subsequently, the mats were used as a label-free electrochemical transducer with a high surface area for biosensing the capture of ZIKV virions. Conductive PVA_Alginate-polyaniline mats helped to transduce the mass changes from the amount of captured ZIKV over the conjugated surface of the ENM into impedimetric changes, thus working as a 3-D biosensor capable of simultaneous sample enrichment and biosensing.

2. EXPERIMENTAL SECTION

2.1. Materials. PVA (M_w 146,000−186,000, 99+% hydrolyzed), sodium alginate, glycine, *N*-(3-dimethylaminopropyl)-*N*′-ethylcarbodiimide (EDC), *N*-hydroxysuccinimide (NHS), ammonium persulfate (APS), glutaraldehyde, morpholino ethanesulfonic acid (MEA), methanol, and hydrochloric acid (HCl) were purchased from Sigma-Aldrich, USA. The polyclonal antibody to ZIKV against the envelope protein produced in rabbit was obtained from GeneTex (Irvine, CA, USA).

ZIKV PE/243, isolated from a ZIKV case diagnosed in the Pernambuco state, Northeast Brazil, was propagated in Vero cells and titrated by the plaque assay as described in a previous publication.[27] In brief, the supernatant was harvested and clarified by centrifugation. ZIKVs were precipitated with 50% polyethylene glycol (PEG 3100) in Dulbecco's modified Eagle's medium (DMEM) and incubated overnight at 4 °C. After centrifugation, the pellet containing the virus particles was resuspended in a mixture of the original supernatant/PEG in DMEM with 25 mM HEPES. The initial concentration was determined to be 1×10^6 plaque forming units (PFU/mL) by the PRNT (results presented in the Supporting Information).

2.2. Electrospinning of PVA_Alginate. The electrospinning conditions were found by a multilevel experimental design presented in the Supporting Information (Tables S1 and S2). A polymeric blend containing 13.34 g of 16% w/w PVA solution and 6.66 g of 2% w/w alginate solution was electrospun for a processing time of 15 h at an injection rate of 1 μL/min at 21 °C and 55% relative humidity. The home-made electrospinning system is composed of a high-voltage power supply, a grounded metallic collector plate covered with aluminum foil, and a cylindrical 14G spinneret connected to a feeding hose coupled to an infusion pump. The electrospinning parameters were optimized to 24 kV and 13 cm distance between the spinneret and the collector plate.

2.3. Stabilization of PVA_Alginate Fibers and Polyaniline Hierarchization. PVA_Alginate ENMs were cross-linked by immersing in a 4 °C methanol solution supplemented with 1% glutaraldehyde and 0.1% HCl. After 72 h, the fibers were removed from the solution, placed in a beaker with Milli-Q water, and set in a shaker at 225 rpm, changing the water from the beaker until no foam

https://doi.org/10.1021/acsami.1c14052
ACS Appl. Mater. Interfaces 2022, 14, 41−48

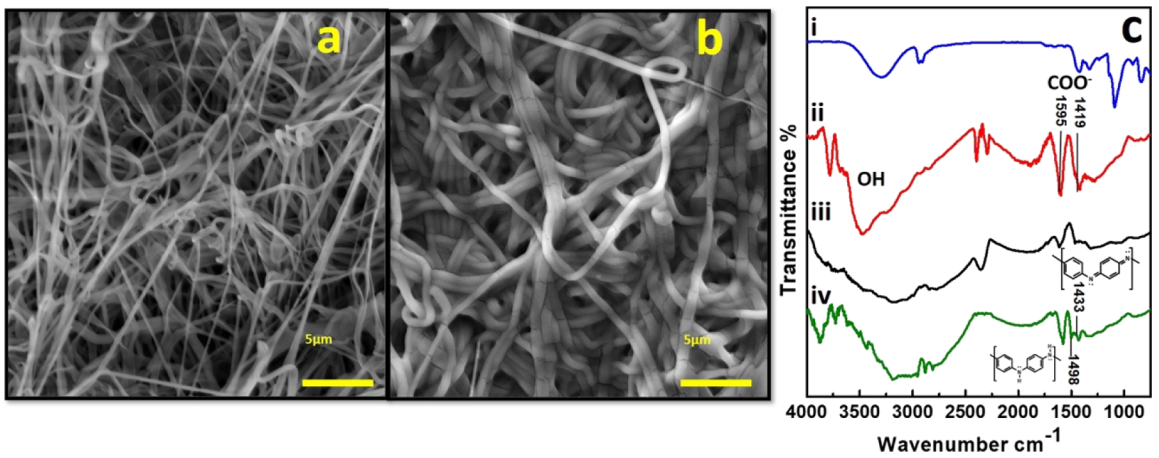

Figure 1. SEM of (a) PVA_Alg nanofibers, (b) PVA_Alg/Pani, and (c) ATR−FTIR analyses of nanofibers performed in between fabrication steps: (i) electrospun pure PVA, (ii) PVA_Alg electrospun blend, (iii) PVA_Alg ENM after cross-linking, and (iv) PVA_Alg/Pani hierarchized ENM.

formation was observed. The ENMs were immersed in an aqueous solution supplemented with 1.5% aniline and 8.3% HCl to achieve hierarchization with polyaniline. After 15 min, an aqueous solution containing 0.76% APS (w/v) and 2.8% HCl was added. The reaction was set in a cooling bath for 12 h at 4 °C. Then, the ENMs were washed by agitation in an orbital shaker at 225 rpm. The water solution was extracted and analyzed by UV−vis spectroscopy using a NanoDrop 2000c spectrophotometer (Thermo Scientific, USA) at 280 nm absorption for protein quantification. The procedure was repeated until zero absorption to avoid signal overlapping.

2.4. Characterization of ENMs. Open porosity represents the average ratio between the volume of pores and the volume of the remaining material in a porous material. In the case of biomedical applications, porosity is a rapidly comparable parameter that is usually calculated through the solvent replacement or gravimetric method.[28] For the calculation, the ENMs were cut into 1 cm^2 squared mats and allowed to dry in a desiccator for 7 days. The fibers were weighed and measured dried, and then they were immediately immersed in water for 12 h to enable their complete hydration. The calculation was performed according to the following equation:[29,30] porosity = $(M_2 - M_1)/\rho V$, where M_1 and M_2 are the mass of the fiber before and after the hydration, respectively, ρ is the absolute density of the hydration solvent, and V is the volume of the hydrated fiber.

The chemical composition of the ENMs was evaluated by attenuated reflectance infrared spectroscopy using an IRTracer-100 spectrophotometer (Shimadzu, Japan) with a zinc selenide crystal (ZnSe) support by measuring the transmittance (% T) from 700 to 4000 cm^{-1} with a 4 cm^{-1} step.

Topography was studied by atomic force microscopy (AFM, Shimadzu SPM-9700) using Tap190Al-G cantilevers (48 N/m and frequency 190 kHz, Budget Sensors, Bulgaria). The morphology was studied with scanning electron microscopy (SEM) using an FEG-SEM MIRA 3 LM (TESCAN, Czech Republic).

2.5. PAb Immobilization. PVA_Alg/Pani mats were stabilized in MEA buffer at pH 3.15 by agitation in an orbital shaker at 225 rpm. Subsequently, the ENMs were functionalized by immersing in a 0.05 M EDC/0.1 M NHS (1:1, v/v) solution (pH 3). After 60 min, they were washed in MEA at pH 3.15 until zero absorption at 280 nm was reached. Afterward, the ENMs were incubated in a 471.8 μg/mL PAbZIKV solution at pH 7.14 and set to shake at 225 rpm. The amount of the tethered antibody was calculated by monitoring the reduction in the protein concentration by UV−vis absorption spectroscopy at 280 nm.

2.6. Capture and Desorption of the Viral Envelope. PVA_Alg/Pani-PAb mats are specific for ZIKV recognition. Each mat was washed in PBS (pH 3) and set to shake at 225 rpm to release any protein adsorbed by non-specific interactions, thereby maintaining only covalently immobilized PAb. The mats were then equilibrated in PBS at pH 7.24 before being exposed to ZIKV samples with an initial concentration of 412.7 μg/mL. ZIKV capture was monitored by UV−vis spectroscopy at 280 nm. After saturation of the mats, desorption was performed by washing PVA_Alg/Pani-PAb-ZIKV mats in a 0.1 M glycine/HCl solution at 2.5, 3.0, and 4.0 pH. Desorption was monitored by UV−vis spectroscopy at 280 nm.

2.7. Electrochemical Impedance Spectroscopy Measurements. All electrochemical measurements were performed in triplicate on a PGSTAT 128 N potentiostat/galvanostat (Metrohm Autolab Inc., The Netherlands) using three electrodes: a platinum counter electrode, a Ag/AgCl reference electrode saturated with KCl solution, and a PVA_Alg-Pani working electrode. Experiments were performed by immersing in PBS (10 mM, pH 7.24) solution. The electrochemical impedance spectroscopy (EIS) response was analyzed with an AC voltage amplitude of 0.01 V at a frequency range of 100 mHz and 100 kHz, and the direct current (dc) potential was set to the open-circuit potential (OCP). Stabilization of OCP E versus time is presented in Supporting Information Figure S1.

3. RESULTS AND DISCUSSION

3.1. Characterization. In Figure 1, we present the morphological and chemical characterization of ENMs. The morphology of an ENM is shown after the cross-linking process (Figure 1a) and hierarchization with polyaniline (Figure 1b). The organization of hierarchized nanofibers changes from thin, separated fibers to an assembly of thickened fibers affixed together in longitudinal arranges. Based on the SEM images, it can be seen that the diameter increases from 0.22 ± 0.088 to 0.72 ± 0.17 μm, with an increase of ∼500 nm in width. FTIR analyses were used to monitor the hierarchization process of the ENMs. In Figure 1C (spectrum i), the spectrum of pure PVA is presented. In Figure 1C (spectrum ii), we observe that the alginate response in the electrospun material overshadows the PVA spectrum, the new peaks at 1595 and 1419 cm^{-1} are related to the symmetric stretching of single-bond COO^- groups,[31] and its presence in the deposited material is demonstrated. After cross-linking (Figure 1C, spectrum iii), it can be observed that the main characteristic bands of the PVA_Alginate pristine blend are maintained. However, in the reticulated membranes, the bands close to 3000 and 3500 cm^{-1} become broadened. These bands are related to the bending vibration of the hydroxyl groups and the linking of hydroxyl groups by hydrogen bonds.[32] Finally, in Figure 1C (spectrum iv), we show the spectrum of ENMs hierarchized with polyaniline. One can observe the characteristic bands at 1433 and 1498 cm^{-1} assigned to the C−C vibrations of polyaniline quinoid and benzoid rings of the

https://doi.org/10.1021/acsami.1c14052
ACS Appl. Mater. Interfaces 2022, 14, 41−48

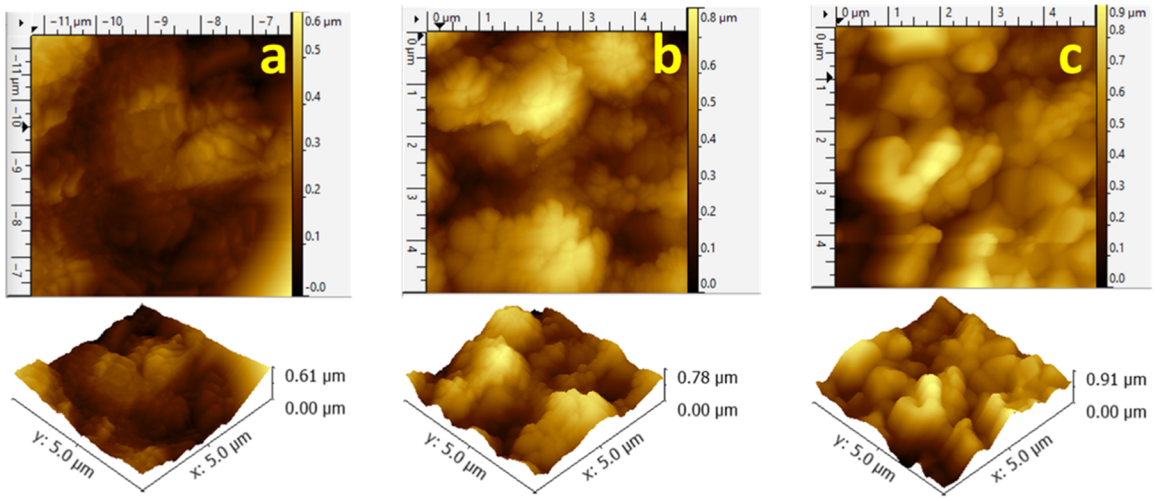

Figure 2. AFM images of ENMs during biofunctionalization and ZIKV capture: (a) PVA_Alg/Pani, (b) antibody immobilization, and (c) ZIKV capture.

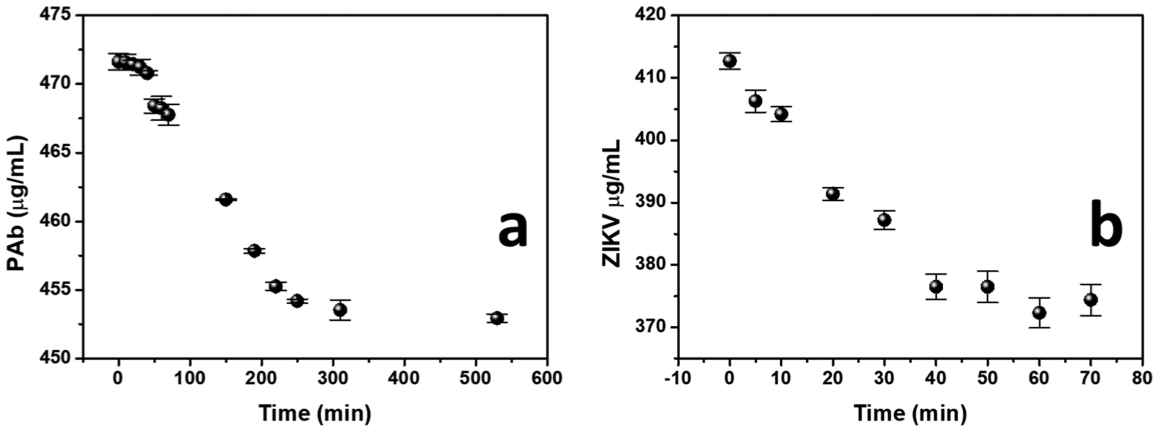

Figure 3. UV−vis measurements performed during (a) covalent bioconjugation of the anti-ZIKV envelope PAb and (b) capture of ZIKV.

emeraldine oxidation state.[33] The available carboxyl sites were estimated *via* the toluidine blue outtake colorimetric assay.[34] Our results showed that the initial concentration was 1.34 mM carboxylic groups available in 14.2 mg (0.25 cm^3) of ENMs.

Alcoholic glutaraldehyde cross-linking treatment provides a bridge between the carboxylic groups of alginate and the hydroxyl groups of PVA, creating an interchain attachment that brings chemical stability and new physicochemical properties to hydrogels.[35] After this treatment, the membranes become porous structures, and after coming in contact with water, they become turgid, increasing their original volume. The ENM porosity was calculated to be 84.42% ± 0.06. This result was expected considering their interaction with water and biocompatibility. For instance, the porosity of polyethersulfone membranes has been calculated to be 71%.[36] This result is important considering that their interaction with water and high porosity can influence higher biocompatibility and hydrophilicity.[37,38]

3.2. Immobilization of PAb and Capture of ZIKV. We investigated the morphological changes of the surface of the hierarchized ENM system by AFM. 3-D 5 × 5 μm images were obtained from the ENM surface before and after PAb immobilization and after interaction with the ZIKV samples. In Figure 2a, we observe the initial topography of the Pani-hierarchized ENM. The covalent bioconjugation between PAb and the terminal carboxyl groups present in the ENM resulted in an accidented topography with pronounced acclivities up to 0.78 μm (Figure 2b). Afterward, ENM_PAbZIKV was exposed to the ZIKV samples. Thus, the success of this process was demonstrated by the transition to a smoother topography and height increase to 0.91 μm. After PAb immobilization, we repeated the colorimetric calculation of carboxyl sites. This time, the result was 3.6 × 10^{-3} mM, a reduction of 99.73%.

The immobilization process of PAbZIKV and later ZIKV capture were also monitored through UV−vis spectroscopy. Figure 3a shows the gradual reduction in protein content from the 471.8 μg/mL PAbZIKV initial solution. The covalent immobilization of the antibody reached 93% completion at 3.3 h (198 min). After that, the immobilization process attained a plateau for 5 h (300 min). After this process, we observed a reduction from 471.6 to 452.9 μg/mL, resulting in 18.7 μg of immobilized PAbZIKV.

Afterward, the capture of ZIKV was tested by immersing the PVA_Alg-Pani-PAb ENM in a 412.7 μg/mL (1 × 10^6 PFU/mL) ZIKV initial solution. In Figure 3b, we present the monitoring of ZIKV capture. It can be observed that the specific capture occurs gradually over a period of 1 h. Passed this time, there is no significant difference in the measurement likely due to PAb probe saturation. It took 40 min to observe a reduction to 376.57 μg/mL. At this point, a plateau was

https://doi.org/10.1021/acsami.1c14052
ACS Appl. Mater. Interfaces 2022, 14, 41−48

attained for 70 min; the minimum observed concentration was 374.47 μg/mL. In total, 38.7 ± 2.5 μg of ZIKV was captured.

Of note, the capture capacity of these novel materials is expected to decrease proportionally to their specificity. For instance, carbonized electrospun polyacrylonitrile membranes have shown unspecific binding capacities in the order of 200 mg/g for the discrimination of proteins based on hydrophobicity/hydrophilicity phenomena.[39] By increasing the selectivity, Ma *et al.* functionalized electrospun polyether sulfone membranes with protein A for their application in the specific purification of IgG from an albumin mixture where they attained a smaller capture capacity of 11.4 μg/mg.[40] In another work, Ma and Ramakrishna functionalized electrospun regenerated cellulose membranes with protein A/G for IG purification, and they reported a capture capacity ranging from 5.6 to 18 μg/mg.[36]

The interaction occurring between the antibody and the viral envelope is based on dissociable physicochemical interactions. For instance, the repulsive and attractive forces involved in antibody−antigen interactions are the same as for other non-covalent protein−protein interactions and thus considered dissociable or weak in this context. As an example, we have electrostatic interactions, dispersion forces, hydrogen bonds, and hydrophobic interactions. Thus, we proceeded to monitor and evaluate the retrieval of ZIKV by washing it from the membrane using glycine solution at different pHs. In Figure 4, we observe that ZIKV is best eluted by using pH 2.5.

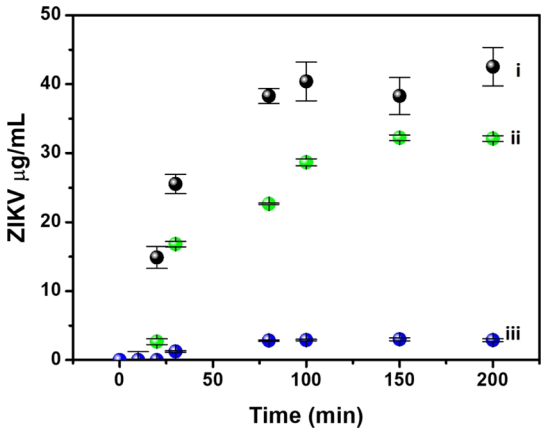

Figure 4. UV−vis measurements performed during the desorption of captured ZIKV in 0.1 M glycine HCl at (i) pH 2.5, (ii) pH 3.0, and (iii) pH 4.0.

The material is less prone to desorption at higher acidities. Thus, the electrostatic interaction at pH 2.5 mostly increases the charge repulsion at the epitope. When the pH increases to 3.0 or above, the antigen−antibody interaction gets stronger. These results demonstrate that the viral recognition can be tuned by varying the pH values according to a previous research, where it has been shown that the pH drives different viral processes. For instance, viral dimer dissociation occurs in acidic pH[41] and triggers ZIKV fusion by the effect of pH alone.[42]

As shown in Figure 4, desorption takes approximately 1.67 h (100 min), and at this time, the calculated desorption was 99.97% (38.29 ± 2.7 μg ZIKV). Once the desorption process is completed, the same membrane was used in the same capture, and the desorption process was performed twice, achieving very similar percentages each time.

Figure 5 shows the monitoring of ZIKV capture and desorption process studied by the EIS technique. This measurement was possible because of the hierarchization of Pani over the ENM. The initial signal measured (a) corresponds to the pristine-hierarchized ENM (PVA_Alg/Pani). After PAb immobilization, the response is (b). At the beginning of the ZIKV capture process, a linear activity can be visualized in the impedimetric response at lower frequencies, indicating the experience of the diffusion process. In general, it was observed that the capture of ZIKV (c−i) resulted in the increase of the size of the semicircle over time, until 70 min of capturing process. The height of the semicircle is related to the quantity of the ZIKV material captured by the functionalized ENM. After washing the PVA_Alg/Pani-PAb-ZIKV ENM for 2 h with a glycine−HCl pH 2.5 solution, the saturated membrane response (i) recedes to (j), very close to the response (b) of the initial hierarchized biosensor containing only PAb. These results confirm the process of PAb immobilization, ZIKV capture, and release observed by UV−vis spectroscopy.

These non-faradaic responses were mathematically fitted to the shape of the deformed semicircles by fine-tuning their electrical response to an equivalent circuit containing elements of the resistance of the electrolytic solution (R_s) and a Warburg impedance (W) joined in parallel to a series of charge-transfer resistance (R_{ct}) and a constant phase element (CPE). The results obtained from the numerical simulation with the equivalent circuit are presented in Table 1. EIS spectra are characterized by the semicircular region representing the charge-transfer resistance (R_{ct}) at the electrical double layer. In Figure 5B, we present the R_{ct} variation percentage of (ΔR_{ct}) described as eq 1

$$\Delta R_{ct}\ (\%) = \frac{R_{ct(EFMPAb\text{-}ZIKV)} - R_{ct(EFMPAb)}}{R_{ct(EFMPab)}} \times 100 \quad (1)$$

$R_{ct(ENMPAb)}$ is the initial response of the PAb-functionalized Pani-hierarchized ENM and $R_{ct(ENMPAb\text{-}ZIKV)}$ is the value calculated at different times after ZIKV capture. Of note, a linear capturing response determined by the equation $y = 115.632 + 7.312x$ with a correlation coefficient (R^2) of 0.92 is obtained during the first 40 min; after this point, a plateau was reached up to 70 min.

With this data, the limit of detection was calculated as LOD = $3.3\sigma/S$, where σ is the SD of the intercept of the regression line and S is the slope of the calibration curve. We found a LOD value of 2.76 μg of ZIKV particles (approximately 6.6×10^3 PFU/mL). Of note, human ZIKV viremia titers range from 10^3 to 10^6 PFU/mL.[43] Therefore, the LOD found is low enough to perform in typical cases, notwithstanding that this self-enriching biosensor can process large amounts of samples until achieving saturation. On the other hand, classical 2D biosensors report LODs around 2×10^{-3} and 5×10^{-2} PFU/mL,[44] certainly below the LOD reported for the molecular technique RT-PCR (337 PFU/mL).[43] However, divergent data regarding the relationship between RNA equivalents and PFU were found, and therefore, further studies are required to discern the effectiveness of these biosensors. For instance, some authors report that 1 PFU equals 2000 RNA copies,[45] 100 RNA copies,[46] and others have calculated 5000 copies.[44]

In order to explore PVA_Alg/Pani-PAb application in real conditions, spiked negative-confirmed blood serum samples were analyzed by EIS. In Figure 6, we present the capture

https://doi.org/10.1021/acsami.1c14052
ACS Appl. Mater. Interfaces 2022, 14, 41−48

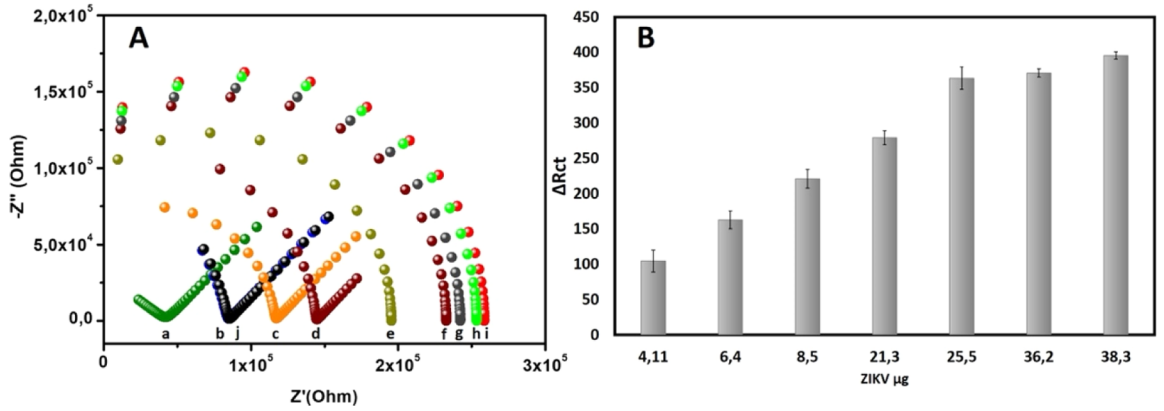

Figure 5. (A) Non-faradaic impedimetric response of (a) pristine PVA_Alg/Pani, (b) PVA_Alg/Pani-PAb, and (c) capture of ZIKV after 1, (d) 5, (e) 10, (f) 20, (g) 30, (h) 40, (i) 70 min, and (j) after ZIKV desorption 200 min processing time. (B) Percentage variation of R_{ct} (ΔR_{ct}) calculated from the equivalent circuit. Three replicates for each concentration were considered for mean value ± standard deviation.

Table 1. Mathematically Fitted Values for the Equivalent Circuit Elements Obtained during the Capture and Elution of ZIKV from ENM-Pani-PAb[a]

electrospun nanofiber mat	CPE (μS)	n	R_{ct} (kΩ)	ΔR_{ct} (%)
ENM-Pani-PAb	4.10 ± 2.14	0.841 ± 0.02	153 ± 0.01	
	ZIKV Capture at Different Times			
1 min	284.8 ± 1.10	0.829 ± 0.01	313 ± 0.01	104.57 ± 15.7
5 min	240.1 ± 2.13	0.837 ± 0.04	402 ± 0.01	162.74 ± 12.4
10 min	227.9 ± 3.25	0.838 ± 0.04	491 ± 0.01	220.91 ± 13.1
20 min	147.2 ± 1.63	0.838 ± 0.03	580 ± 0.01	279.08 ± 9.5
30 min	72.9 ± 2.33	0.738 ± 0.05	709 ± 0.01	363.39 ± 15.8
40 min	73.4 ± 1.15	0.729 ± 0.01	720 ± 0.01	370.58 ± 5.8
70 min	68.9 ± 2.83	0.737 ± 0.04	758 ± 0.01	395.42 ± 5.4

[a]Triplicates for each experimental condition were used as the mean value ± standard deviation.

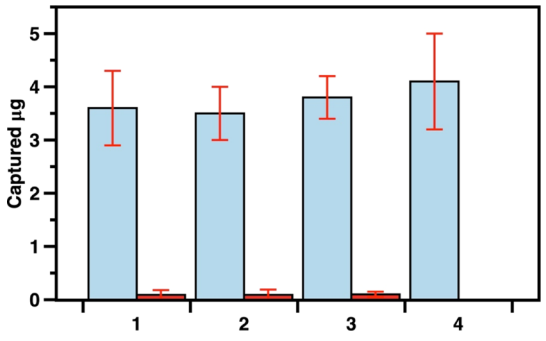

Figure 6. Impedimetric calculations of captured ZIKV or DENV2 virus in 10 mL of spiked negative-confirmed serum samples.

results calculated through EIS detection. In total, four samples spiked with ZIKV and three with dengue virus (DENV2) were analyzed. However, because of the interference found in the concentrated blood serum, before spiking the samples with 4 μg of ZIKV (1×10^3 PFU) or 4 μg of DENV2, the sera were diluted at 10% in PBS pH 7.24 10 mM, and therefore, its volume increased 10 times. All 10 mL of diluted volume was tested with the same ENM. This time, in the presence of blood sera, we found that after 70 min, we achieved to capture 3.75 ± 0.6 μg of ZIKV (approximately 94% of the total sample). DENV2 capture was negligible (0.09 ± 0.0503 μg). After this time, no further changes were noticed. These results demonstrate the specificity and reusability of the 3-D biosensor. To the best of our knowledge, the PVA_Alg/Pani ENM is a novel approach that allows the enrichment of the samples while simultaneously monitoring the completion of the capture and elution processes by EIS. We propose this application as an excellent alternative to diagnose samples with small amounts of target analytes. Patients in different stages of infection can be better assisted with efficient and low-cost detection of ZIKV, overcoming the disadvantages of conventional methodologies.

4. CONCLUSIONS

An asymmetrical nanofiber-based mat with a 3-D open-porous characteristic was produced through the electrospinning of PVA and alginate polymers and posterior hierarchization with conductive polyaniline. Polyclonal anti-ZIKV envelope antibodies were covalently immobilized as probes to capture the ZIKV present in the Vero cell culture broth. The capture of 38.7 ± 2.5 μg ZIKV and the elution of 99% were successfully achieved. As a result of the covalent immobilization of PAb, the capture−elution features of the system remained up to 90% after being reused several times. The processing of biological samples was monitored by UV−vis spectroscopy. Because of polyaniline conductive properties, EIS monitoring was enabled as well. Despite its high porosity (84%), the hierarchized ENM showed low binding efficiency, attributed to the high specificity of its ligand−ligate pair model (PAbZIKV-ZIKV). Its specificity and reusability were tested in real conditions by processing 10 mL of ZIKV- or DENV-spiked serum samples. The capture ability dropped to approximately 94% of the total sample. However, because of its demonstrated abilities, the system is proposed as a fast small-scale purification system that

https://doi.org/10.1021/acsami.1c14052
ACS Appl. Mater. Interfaces 2022, 14, 41−48

can be simultaneously monitored electrochemically and optically.

■ ASSOCIATED CONTENT

Supporting Information

The Supporting Information is available free of charge at https://pubs.acs.org/doi/10.1021/acsami.1c14052.

Factorial and multilevel experimental designs for the optimization of ENM, OCP of ENM, and PRNT for ZIKV neutralization by anti-ZIKV antibodies (PDF)

■ AUTHOR INFORMATION

Corresponding Author

Cesar A. S. Andrade − *Therapeutic Innovation Program and Biochemistry Department, Federal University of Pernambuco, Recife 50670-901, Brazil;* orcid.org/0000-0002-3271-2817; Phone: +55-81-2126-8450; Email: cesar.sandrade@ufpe.br; Fax: +55-81-2126-8547

Authors

Isaac A. M. Frias − *Therapeutic Innovation Program and Biochemistry Department, Federal University of Pernambuco, Recife 50670-901, Brazil*

Laura Helena Vega Gonzales Gil − *Institute Aggeu Magalhães (IAM), Oswaldo Cruz Foundation (Fiocruz), Recife 21040-900, Brazil*

Marli T. Cordeiro − *Institute Aggeu Magalhães (IAM), Oswaldo Cruz Foundation (Fiocruz), Recife 21040-900, Brazil*

Maria D. L. Oliveira − *Therapeutic Innovation Program and Biochemistry Department, Federal University of Pernambuco, Recife 50670-901, Brazil*

Complete contact information is available at: https://pubs.acs.org/10.1021/acsami.1c14052

Author Contributions

This manuscript was written through contributions from all authors. All authors have given approval to the final version of the manuscript. I.A.M.F. contributed to methodology, validation, formal analysis, investigation, data curation, and writing—original draft. L.H.V.G.G. contributed to visualization. M.T.C. contributed to visualization. M.D.L.O. contributed to review and editing and funding acquisition. C.A.S.A. contributed to supervision, review and editing, and funding acquisition.

Funding

The authors are grateful for the support from the Brazilian National Council of Scientific and Technological Development/CNPq (grant numbers 314894/2018-7, 314756/2018-3, and 435059/2018-1) and the Science and Technology Support Foundation of Pernambuco State/FACEPE (BCT-0056-2.09/18). Isaac A. M. Frías would like to thank the Coordination for the Improvement of Higher Education Personnel CAPES and FACEPE for the postdoctoral fellowship (APQ-0437-4.03/17). We thank Prof. Celso P. de Melo (Physics department, UFPE) for making available the UV−vis equipment for optical analysis and Prof. Abdelhamid Errachid (UCBL1 Lyon, France) for making available the electrospinning and electrochemical equipment for supplementary measurements.

Notes

The authors declare no competing financial interest.

■ REFERENCES

(1) Alera, M. T.; Hermann, L.; Tac-An, I. A.; Klungthong, C.; Rutvisuttinunt, W.; Manasatienkij, W.; Villa, D.; Thaisomboonsuk, B.; Velasco, J. M.; Chinnawirotpisan, P.; Lago, C. B.; Roque, V. G., Jr.; Macareo, L. R.; Srikiatkhachorn, A.; Fernandez, S.; Yoon, I. K. Zika virus infection, Philippines, 2012. *Emerg. Infect. Dis.* **2015**, *21*, 722.

(2) Gallichotte, E. N.; Young, E. F.; Baric, T. J.; Yount, B. L.; Metz, S. W.; Begley, M. C.; de Silva, A. M.; Baric, R. S. Role of Zika Virus Envelope Protein Domain III as a Target of Human Neutralizing Antibodies. *mBio* **2019**, *10*, No. e01485.

(3) Leung, G. H. Y.; Baird, R. W.; Druce, J.; Anstey, N. M. Zika Virus Infection in Australia Following a Monkey Bite in Indonesia. *Southeast Asian J. Trop. Med. Publ. Health* **2015**, *46*, 460.

(4) Oliveira Melo, A. S.; Malinger, G.; Ximenes, R.; Szejnfeld, P. O.; Alves Sampaio, S.; Bispo de Filippis, A. M. Zika Virus Intrauterine Infection Causes Fetal Brain Abnormality and Microcephaly: Tip of the Iceberg? *Ultrasound Obstet. Gynecol.* **2016**, *47*, 6−7.

(5) Niu, X.; Yan, Q.; Yao, Z.; Zhang, F.; Qu, L.; Wang, C.; Wang, C.; Lei, H.; Chen, C.; Liang, R.; Luo, J.; Wang, Q.; Zhao, L.; Zhang, Y.; Luo, K.; Wang, L.; Wu, H.; Liu, T.; Li, P.; Zheng, Z.; Tan, Y. J.; Feng, L.; Zhang, Z.; Han, J.; Zhang, F.; Chen, L. Longitudinal Analysis of the Antibody Repertoire of a Zika Virus-Infected Patient Revealed Dynamic Changes in Antibody Response. *Emerg. Microb. Infect.* **2020**, *9*, 111−123.

(6) Priyamvada, L.; Suthar, M. S.; Ahmed, R.; Wrammert, J. Humoral Immune Responses against Zika Virus Infection and the Importance of Preexisting Flavivirus Immunity. *J. Infect. Dis.* **2017**, *216*, S906−S911.

(7) Poland, G. A.; Kennedy, R. B.; Ovsyannikova, I. G.; Palacios, R.; Ho, P. L.; Kalil, J. Development of Vaccines against Zika Virus. *Lancet Infect. Dis.* **2018**, *18*, e211−e219.

(8) Lanciotti, R. S.; Kosoy, O. L.; Laven, J. J.; Velez, J. O.; Lambert, A. J.; Johnson, A. J.; Stanfield, S. M.; Duffy, M. R. Genetic and Serologic Properties of Zika Virus Associated with an Epidemic, Yap State, Micronesia, 2007. *Emerg. Infect. Dis.* **2008**, *14*, 1232−1239.

(9) Villamil-Gómez, W. E.; González-Camargo, O.; Rodriguez-Ayubi, J.; Zapata-Serpa, D.; Rodriguez-Morales, A. J. Dengue, Chikungunya and Zika Co-Infection in a Patient from Colombia. *J. Infect. Pub. Health* **2016**, *9*, 684.

(10) Faccini-Martínez, Á. A.; Botero-García, C. A.; Benítez-Baracaldo, F. C.; Pérez-Díaz, C. E. With Regard about the Case of Dengue, Chikungunya and Zika Co-Infection in a Patient from Colombia. *J. Infect. Publ. Health* **2016**, *9*, 687.

(11) Alam, M. A.; Hasan, M. R.; Anzar, N.; Suleman, S.; Narang, J. Diagnostic approaches for the rapid detection of Zika virus-A review. *Process Biochem.* **2021**, *101*, 156−168.

(12) Afsahi, S.; Lerner, M. B.; Goldstein, J. M.; Lee, J.; Tang, X.; Bagarozzi, D. A.; Pan, D.; Locascio, L.; Walker, A.; Barron, F.; Goldsmith, B. R. Novel Graphene-Based Biosensor for Early Detection of Zika Virus Infection. *Biosens. Bioelectron.* **2018**, *100*, 85−88.

(13) Corman, V. M.; Rasche, A.; Baronti, C.; Aldabbagh, S.; Cadar, D.; Reusken, C. B.; Pas, S. D.; Goorhuis, A.; Schinkel, J.; Molenkamp, R.; Kümmerer, B. M.; Bleicker, T.; Brünink, S.; Eschbach-Bludau, M.; Eis-Hübinger, A. M.; Koopmans, M. P.; Schmidt-Chanasit, J.; Grobusch, M. P.; de Lamballerie, X.; Drosten, C.; Drexler, J. F. Assay Optimization for Molecular Detection of Zika Virus. *Bull. World Health Organ.* **2016**, *94*, 880.

(14) Singh, S.; Noori, M. T.; Verma, N. Efficient Bio-Electro-reduction of CO2 to Formate on a Iron Phthalocyanine-Dispersed CDC in Microbial Electrolysis System. *Electrochim. Acta* **2020**, *338*, 135887.

(15) Singh, S.; Pophali, A.; Omar, R. A.; Kumar, R.; Kumar, P.; Mondal, D. P.; Pant, D.; Verma, N. A Nickel Oxide-Decorated in Situ Grown 3-D Graphitic Forest Engrained Carbon Foam Electrode for Microbial Fuel Cells. *Chem. Commun.* **2021**, *57*, 879−882.

(16) Pophali, A.; Singh, S.; Verma, N. A Dual Photoelectrode-Based Double-Chambered Microbial Fuel Cell Applied for Simultaneous

COD and Cr (VI) Reduction in Wastewater. *Int. J. Hydrogen Energy* **2021**, *46*, 3160−3170.
(17) Amouzadeh Tabrizi, M.; Ferré-Borrull, J.; Marsal, L. F. Remote Biosensor for the Determination of Trypsin by Using Nanoporous Anodic Alumina as a Three-Dimensional Nanostructured Material. *Sci. Rep.* **2020**, *10*, 2356.
(18) Ma, Y.; Liu, N.; Xu, Z.; Wang, J.; Luo, X. An Ultrasensitive Biosensor Based on Three-Dimensional Nanoporous Conducting Polymer Decorated with Gold Nanoparticles for MicroRNA Detection. *Microchem. J.* **2021**, *161*, 105780.
(19) Xu, L.-H.; Li, J.-j.; Zeng, H.-B.; Zhang, X.-J.; Cosnier, S.; Marks, R. S.; Shan, D. ATMP-Induced Three-Dimensional Conductive Polymer Hydrogel Scaffold for a Novel Enhanced Solid-State Electrochemiluminescence Biosensor. *Biosens. Bioelectron.* **2019**, *143*, 111601.
(20) Ramakrishna, S.; Fujihara, K.; Teo, W.-E.; Yong, T.; Ma, Z.; Ramaseshan, R. Electrospun Nanofibers: Solving Global Issues. *Mater. Today* **2006**, *9*, 40−50.
(21) Yew, C.; Azari, P.; Choi, J.; Muhamad, F.; Pingguan-Murphy, B. Electrospun Polycaprolactone Nanofibers as a Reaction Membrane for Lateral Flow Assay. *Polymers* **2018**, *10*, 1387.
(22) Lai, Y.-C.; Chang, Y.-R.; Chen, M.-L.; Lo, Y.-K.; Lai, J.-Y.; Lee, D.-J. Poly(Vinyl Alcohol) and Alginate Cross-Linked Matrix with Immobilized Prussian Blue and Ion Exchange Resin for Cesium Removal from Waters. *Bioresour. Technol.* **2016**, *214*, 192−198.
(23) Mahdavinia, G. R.; Mousanezhad, S.; Hosseinzadeh, H.; Darvishi, F.; Sabzi, M. Magnetic Hydrogel Beads Based on PVA/Sodium Alginate/Laponite RD and Studying Their BSA Adsorption. *Carbohydr. Polym.* **2016**, *147*, 379−391.
(24) Wróblewska-Krepsztul, J.; Rydzkowski, T.; Michalska-Pożoga, I.; Thakur, V. K. Biopolymers for Biomedical and Pharmaceutical Applications: Recent Advances and Overview of Alginate Electrospinning. *Nanomaterials* **2019**, *9*, 404.
(25) Yang, J. M.; Yang, J. H.; Tsou, S. C.; Ding, C. H.; Hsu, C. C.; Yang, K. C.; Yang, C. C.; Chen, K. S.; Chen, S. W.; Wang, J. S. Cell Proliferation on PVA/Sodium Alginate and PVA/Poly(γ-Glutamic Acid) Electrospun Fiber. *Mater. Sci. Eng., C* **2016**, *66*, 170−177.
(26) Kurimoto, R.; Namekawa, K.; Ellis, A. V.; Naito, M.; Ebara, M. Selective Adsorption of Globulin on Nanofiber Meshes for Immunoadsorption Therapy. *New J. Chem.* **2018**, *42*, 2916−2922.
(27) Castanha, P. M. S.; Nascimento, E. J. M.; Braga, C.; Cordeiro, M. T.; de Carvalho, O. V.; de Mendonça, L. R.; Azevedo, E. A. N.; França, R. F. O.; Dhalia, R.; Marques, E. T. A. Dengue Virus−Specific Antibodies Enhance Brazilian Zika Virus Infection. *J. Infect. Dis.* **2016**, *215*, 781−785.
(28) Sun, X.; Uyama, H. A Poly (Vinyl Alcohol)/Sodium Alginate Blend Monolith with Nanoscale Porous Structure. *Nanoscale Res. Lett.* **2013**, *8*, 411.
(29) Shabir, F.; Erum, A.; Tulain, U. R.; Hussain, M. A.; Ahmad, M.; Akhter, F. Preparation and Characterization of PH Sensitive Crosslinked Linseed Polysaccharides-Co-Acrylic Acid/Methacrylic Acid Hydrogels for Controlled Delivery of Ketoprofen. *Des. Monomers Polym.* **2017**, *20*, 485−495.
(30) Lin, W.-J.; Lu, C.-H. Characterization and permeation of microporous poly(ε-caprolactone) films. *J. Membr. Sci.* **2002**, *198*, 109−118.
(31) Hajiali, H.; Heredia-Guerrero, J. A.; Liakos, I.; Athanassiou, A.; Mele, E. Alginate Nanofibrous Mats with Adjustable Degradation Rate for Regenerative Medicine. *Biomacromolecules* **2015**, *16*, 936−943.
(32) Kyzioł, A.; Michna, J.; Moreno, I.; Gamez, E.; Irusta, S. Preparation and Characterization of Electrospun Alginate Nanofibers Loaded with Ciprofloxacin Hydrochloride. *Eur. Polym. J.* **2017**, *96*, 350−360.
(33) Bhadra, J.; Al-Thani, N. Advances in Blends Preparation Based on Electrically Conducting Polymer. *Emergent Mater.* **2019**, *2*, 67−77.
(34) Sano, S.; Kato, K.; Ikada, Y. Introduction of Functional Groups onto the Surface of Polyethylene for Protein Immobilization. *Biomaterials* **1993**, *14*, 817−822.
(35) Mohammadi, S.; Ramakrishna, S.; Laurent, S.; Shokrgozar, M. A.; Semnani, D.; Sadeghi, D.; Bonakdar, S.; Akbari, M. Fabrication of Nanofibrous PVA/Alginate-Sulfate Substrates for Growth Factor Delivery. *J. Biomed. Mater. Res., Part A* **2019**, *107*, 403−413.
(36) Ma, Z.; Ramakrishna, S. Electrospun Regenerated Cellulose Nanofiber Affinity Membrane Functionalized with Protein A/G for IgG Purification. *J. Membr. Sci.* **2008**, *319*, 23−28.
(37) Ameer, J. M.; Pr, A. K.; Kasoju, N. Strategies to Tune Electrospun Scaffold Porosity for Effective Cell Response in Tissue Engineering. *J. Funct. Biomater.* **2019**, *10*, 30.
(38) Chen, H.-W.; Lin, M.-F. Characterization, Biocompatibility, and Optimization of Electrospun SF/PCL/CS Composite Nanofibers. *Polymers* **2020**, *12*, 1439.
(39) Schneiderman, S.; Zhang, L.; Fong, H.; Menkhaus, T. J. Surface-Functionalized Electrospun Carbon Nanofiber Mats as an Innovative Type of Protein Adsorption/Purification Medium with High Capacity and High Throughput. *J. Chromatogr. A* **2011**, *1218*, 8989−8995.
(40) Ma, Z.; Lan, Z.; Matsuura, T.; Ramakrishna, S. Electrospun Polyethersulfone Affinity Membrane: Membrane Preparation and Performance Evaluation. *J. Chromatogr. B: Anal. Technol. Biomed. Life Sci.* **2009**, *877*, 3686−3694.
(41) Modis, Y.; Ogata, S.; Clements, D.; Harrison, S. C. Structure of the Dengue Virus Envelope Protein after Membrane Fusion. *Nature* **2004**, *427*, 313−319.
(42) Rawle, R. J.; Webster, E. R.; Jelen, M.; Kasson, P. M.; Boxer, S. G. PH Dependence of Zika Membrane Fusion Kinetics Reveals an Off-Pathway State. *ACS Cent. Sci.* **2018**, *4*, 1503−1510.
(43) Faye, O.; Faye, O.; Dupressoir, A.; Weidmann, M.; Ndiaye, M.; Alpha Sall, A. One-Step RT-PCR for Detection of Zika Virus. *J. Clin. Virol.* **2008**, *43*, 96−101.
(44) Tancharoen, C.; Sukjee, W.; Thepparit, C.; Jaimipuk, T.; Auewarakul, P.; Thitithanyanont, A.; Sangma, C. Electrochemical Biosensor Based on Surface Imprinting for Zika Virus Detection in Serum. *ACS Sens.* **2019**, *4*, 69−75.
(45) Priye, A.; Bird, S. W.; Light, Y. K.; Ball, C. S.; Negrete, O. A.; Meagher, R. J. A Smartphone-Based Diagnostic Platform for Rapid Detection of Zika, Chikungunya, and Dengue Viruses. *Sci. Rep.* **2017**, *7*, 44778.
(46) Xu, M.-Y.; Liu, S.-Q.; Deng, C.-L.; Zhang, Q.-Y.; Zhang, B. Detection of Zika Virus by SYBR Green One-Step Real-Time RT-PCR. *J. Virol. Methods* **2016**, *236*, 93−97.

https://doi.org/10.1021/acsami.1c14052
ACS Appl. Mater. Interfaces 2022, 14, 41−48